




Low-temperature sintering PZT-based ceramics for extreme condition application

Haiying Li¹, Bijun Fang^{1,*} , Shuai Zhang¹, Xiaolong Lu¹, and Jianning Ding^{1,2,*}

¹ School of Materials Science and Engineering, Jiangsu Collaborative Innovation Center of Photovoltaic Science and Engineering, Jiangsu Province Cultivation Base for State Key Laboratory of Photovoltaic Science and Technology, National Experimental Demonstration, Center for Materials Science and Engineering, Changzhou University, Changzhou 213164, China

² School of Mechanical Engineering, Yangzhou University, Yangzhou 225127, China

Received: 20 June 2023

Accepted: 28 September 2023

Published online:
7 October 2023

© The Author(s), under exclusive licence to Springer Science+Business Media, LLC, part of Springer Nature, 2023

ABSTRACT

Ba(Cu_{0.5}W_{0.5})O₃ (BaCW)-doped (1-x)Pb(Zr_{0.5}Ti_{0.5})O₃-x(Bi_{0.5}Na_{0.5})ZrO₃ [(1-x)PZT-xBNZ, x = 0.025–0.1] ceramics were prepared by solid-state reaction method. Low-temperature sintering is realized at around 1000 °C sintering temperature due to adding BaCW sintering aid and (Bi_{0.5}Na_{0.5})ZrO₃ (BNZ) second component. All low-temperature sintered BaCW-doped (1-x)PZT-xBNZ ceramics exhibit pure perovskite structure, in which the structure changes successively from tetragonal, across morphotropic phase boundary (MPB) and to rhombohedral with increasing the BNZ content. All samples have large density, high resistivity, and rather uniform morphology with decreased grain size. All ceramics present apparent relaxation characteristic, and the MPB effect is confirmed by dielectric, ferroelectric, and piezoelectric performance characterization, whereas extremum performance appears at different compositions. High Curie temperature (T_C) with acceptable piezoelectricity (d_{33}) is obtained in the BaCW-doped (1-x)PZT-xBNZ system prepared by low-temperature sintering technique, i.e., the 1000 °C sintered 2 wt% BaCW-doped 0.9PZT-0.1BNZ having $d_{33} = 209$ pC/N with $T_C = 281$ °C, and 0.95PZT-0.05BNZ having $d_{33} = 151$ pC/N with $T_C = 345$ °C, which present broad application possibility in piezoelectric-related fields under extreme condition.

1 Introduction

Because of low Curie temperature (T_C), inferior piezoelectric performance, high sintering temperature, etc., of lead-free piezoelectric materials [1–3], Pb(Zr,Ti)O₃ (PZT)-based piezoelectric ceramics have still dominated applications in piezoelectric components due to the superior comprehensive performance [4]. The progress in technology and society has triggered many

novel application fields, such as metallurgy, aerospace, oil and gas exploration, in which extreme working condition requires high T_C piezoelectric materials [5]. Due to the existence of depolarization phenomenon and low-temperature ferroelectric phase transition [6, 7], safe working temperature of piezoelectric materials is far less than the corresponding T_C temperature [8], which stimulates enthusiastic interest in searching high T_C piezoelectric materials.

Address correspondence to E-mail: fangbj@cczu.edu.cn; dingjn@cczu.edu.cn

Besides developing novel compositions [9–11], PZT still attracts our interest due to scale production, widespread application, and cost considerations. Based on the study of morphotropic phase boundary (MPB), normally representing coexistence region of rhombohedral phase and tetragonal phase [10], $\text{Pb}(\text{Zr}_{0.5}\text{Ti}_{0.5})\text{O}_3$ was selected as matrix in this work, in which Ti content was slightly larger than the MPB region, and could increase T_C temperature [12].

$\text{Pb}(\text{Zr}_{0.5}\text{Ti}_{0.5})\text{O}_3$ deviates from the MPB region slightly, its structure approaches tetragonal phase, and its electrical performance decreases but has slightly higher T_C temperature, which requires further adjustment. Constructing MPB is still a useful method to increase electrical properties in developing novel ferroelectric materials [12–14], where $(\text{Bi}_{0.5}\text{Na}_{0.5})\text{ZrO}_3$ was chosen as a second component in this work, which could also help decrease sintering temperature due to low melting point of Bi-based oxide [15]. $(\text{Bi}_{0.5}\text{Na}_{0.5})\text{ZrO}_3$ is similar to the well-known $(\text{Bi}_{0.5}\text{Na}_{0.5})\text{TiO}_3$, in which Ti and Zr have similar outer electron orbit, and Zr will affect ion interaction force and polarization state due to difference of atomic orbital number [16–19]. Lv et al. studied the role of $\text{Bi}_{0.5}\text{A}_{0.5}\text{ZrO}_3$ ($A = \text{K}, \text{Na}, \text{Ag}, \text{and } (\text{Na}0.82\text{K}0.18)$) on the potassium sodium niobate (KNN) ceramics, and found that Zr^{4+} acted as a buffer, Bi^{3+} was an accelerator, and A^+ acted as a stabilizer. The synergetic effects reduced the orthorhombic–tetragonal phase transition, providing a novel strategy to design phase boundary in KNN without destroying long-range ordering [17]. Then, pseudo-binary solid solution $\text{Pb}(\text{Zr}_{0.5}\text{Ti}_{0.5})\text{O}_3\text{--}(\text{Bi}_{0.5}\text{Na}_{0.5})\text{ZrO}_3$ could be formed, and stabilized perovskite structure and improved electrical performance could be anticipated.

Ceramic processing and physical performance have closed relationship [20], in which sintering temperature is very important for preparing lead-based ceramics. The sintering temperature of preparing the PZT-based piezoelectric ceramics is relatively high, usually 1250 °C or above [21]. In a recent work reported by Lin et al., in order to obtain large transduction coefficient and high T_C temperature in PZT, the sintering temperature was still as high as 1180 °C to prepare the $(\text{Pb}_{1-x}\text{Bi}_x)((\text{Zr}_{0.53}\text{Ti}_{0.47})_{1-x}\text{Fe}_x)\text{O}_3$ ceramics even though co-doped Bi_2O_3 and Fe_2O_3 [22]. Such high sintering temperature not only causes severe evaporation of Pb during sintering, leading to reduce phase purity and deteriorate electrical properties, but also endangers health and pollutes environment [23].

Low-temperature sintering technique provides a possibility to solve such dilemma. To realize low-temperature sintering, besides adding low melting point second component, such as $(\text{Bi}_{0.5}\text{Na}_{0.5})\text{ZrO}_3$ [18, 19], and obtaining high sintering active precursor powder via liquid method [24–26], adding appropriate sintering aid is mostly used method and is very effective to decrease sintering temperature [27, 28]. $\text{Ba}(\text{Cu}_{0.5}\text{Wu}_{0.5})\text{O}_3$ (BaCW) is a perovskite structure sintering aid and has been used in lead-free system [29, 30]. Wang et al. reported adding 0–6 mol% $\text{Ba}(\text{Cu}_{1/2}\text{W}_{1/2})\text{O}_3$ into the $(\text{Bi}_{1/2}\text{Na}_{1/2})\text{TiO}_3$ ceramics, and densified ceramics were sintered at 1130 °C. The addition of BaCW facilitated poling process, and improved piezoelectric performance and decreased dielectric loss with minor impure phase were achieved at appropriate doping amount [29]. Li et al. investigated low-temperature sintering of the $(\text{Ba}_{0.85}\text{Ca}_{0.15})(\text{Zr}_{0.1}\text{Ti}_{0.9})\text{O}_3$ ceramics by $\text{Ba}(\text{Cu}_{0.5}\text{Wu}_{0.5})\text{O}_3$ addition, and the sintering temperature was reduced from 1540 to 1350 °C. At small BaCW doping amount, sintering ability was improved, high piezoelectricity was retained, and the T_C temperature was increased slightly [30].

In this paper, $\text{Ba}(\text{Cu}_{0.5}\text{Wu}_{0.5})\text{O}_3$ (BaCW) was used as sintering aid, which was expected that not only realized low-temperature sintering in the $(1-x)\text{Pb}(\text{Zr}_{0.5}\text{Ti}_{0.5})\text{O}_3\text{--}x(\text{Bi}_{0.5}\text{Na}_{0.5})\text{ZrO}_3$ [$(1-x)\text{PZT--}x\text{BNZ}$] ceramics, but also affected crystal structure and electrical performance due to the tetragonal perovskite structure of BaCW [29, 30]. This work would verify that BaCW could also promote sintering capability in lead-containing system. However, both BNZ second component and BaCW sintering aid could decrease sintering temperature and T_C temperature simultaneously. Then, it was necessary to find a balance between increasing T_C temperature to satisfy requirement of extreme condition application and decreasing sintering temperature to facilitate ceramic processing.

The strategy of adding Bi-based second component and BaCW sintering aid can decrease sintering temperature, avoid evaporation of Pb, and save energy, presenting possibility to obtain high T_C and high-performance piezoelectric ceramics and prospect application in multi-layer co-sintered ceramic industry where low-cost silver electrode was recommended first as inner electrode [31]. Therefore, low-temperature densified sintering at around 1000 °C was realized in the $(1-x)\text{PZT--}x\text{BNZ}$ system due to adding BNZ second component and BaCW sintering aid. The 1000 °C sintered 2 wt% BaCW-doped 0.95PZT–0.05BNZ and

0.9PZT–0.1BNZ ceramics have high T_C temperature and acceptable piezoelectricity, presenting broad application prospect in high-temperature piezoelectric-related fields under extreme condition.

2 Experimental procedure

$(1-x)\text{Pb}(\text{Zr}_{0.5}\text{Ti}_{0.5})\text{O}_3-x(\text{Bi}_{0.5}\text{Na}_{0.5})\text{ZrO}_3$ [(1-x)PZT–xBNZ, $x = 0.025, 0.05, 0.075, 0.1$] ceramics were prepared by low-temperature sintering technique using $\text{Ba}(\text{Cu}_{0.5}\text{Wu}_{0.5})\text{O}_3$ (BaCW) as sintering aid. High purity PbO , ZrO_2 , TiO_2 , Bi_2O_3 , Na_2CO_3 , BaCO_3 , CuO , and WO_3 were used as raw materials. After fully drying, stoichiometric weighing, and well mixing, perovskite precursor powder (1-x)PZT–xBNZ was prepared by calcining well mixed stoichiometrically weighed PbO , ZrO_2 , TiO_2 , Bi_2O_3 , and Na_2CO_3 at 775 °C for 2 h, and perovskite sintering aid BaCW was prepared by calcining well mixed stoichiometrically weighed BaCO_3 , CuO , and WO_3 at 870 °C for 2 h, separately. To fully utilize promoting sintering effect of sintering aid, BaCW was added into the calcined (1-x)PZT–xBNZ precursor powder before granulation and pressing into circular green pellets. In order to achieve goal of 1000 °C low-temperature sintering, 2 or 2.5 wt% calcined BaCW powder was added. Such doping amount was selected since when the BaCW doping amount was too low, the sintering temperature could not be decreased to around 1000 °C; when the BaCW doping amount was too large, the dielectric loss was unacceptable large. Sintering process was undertaken at sintering temperature of 980–1010 °C and soaking time of 2 h, after separate burning out of polyvinyl alcohol binder at 600 °C for 2 h.

Crystal structure and free-surface morphology were characterized by Rigaku D/max-2500/PC X-ray diffractometer (XRD) and JEOL JSM-6510 scanning electron microscopy (SEM), respectively, using well-ground BaCW-doped (1-x)PZT–xBNZ ceramics. High-temperature silver electrode was formed by manually coated with silver paste and fired at 850 °C for 0.5 h. Based on which, room-temperature resistance was measured using Agilent 4339B Meter, dielectric performance-temperature relationship was measured by Partulab HDMS-1000 measurement system, room-temperature ferroelectric properties were measured using Radiant Precision Premier LC II, and piezoelectric properties were measured by ZJ-6 A meter and TH2826 LCR

Meter after poling in silicone oil for 1 min at room temperature under several electric field [32].

3 Results and discussion

3.1 Structure change and density analysis

In this work, (1-x)PZT–xBNZ composition and BaCW doping amount are 2 studied variables, and sintering temperature no higher than 1000 °C with acceptable densification is pursued goal. Based on preliminary experiments, 2 and 2.5 wt% BaCW doping amount are selected, and the influence on sintering behavior of 0.975PZT–0.025BNZ and 0.95PZT–0.05BNZ is analyzed by XRD measurement as shown in Figs. 1 and 2. All sintered ceramics

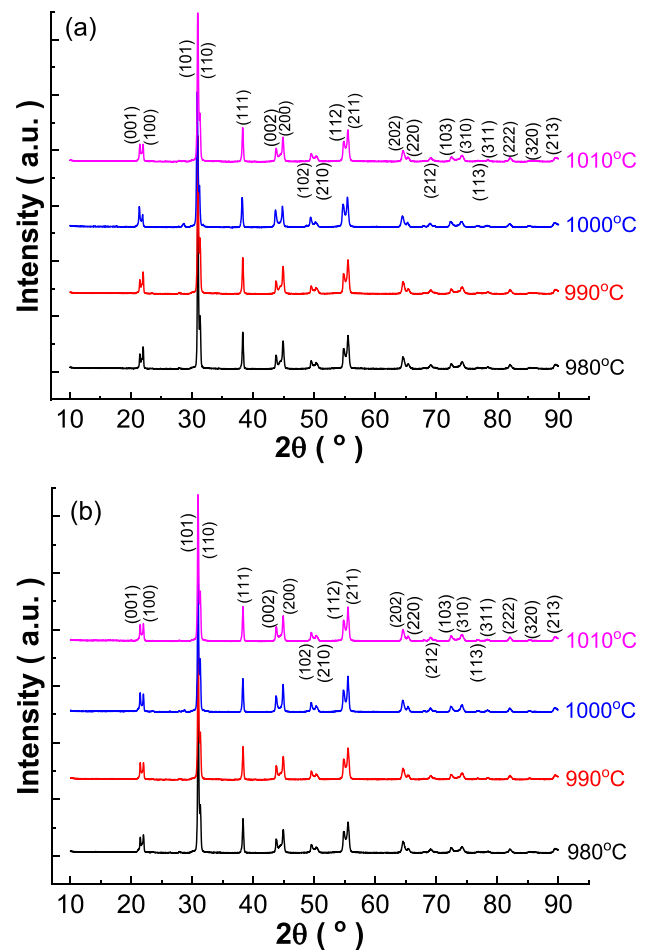


Fig. 1 XRD patterns of BaCW-doped 0.975PZT–0.025BNZ ceramics sintered at low temperatures. **a** 2 wt% BaCW doping; **b** 2.5 wt% BaCW doping

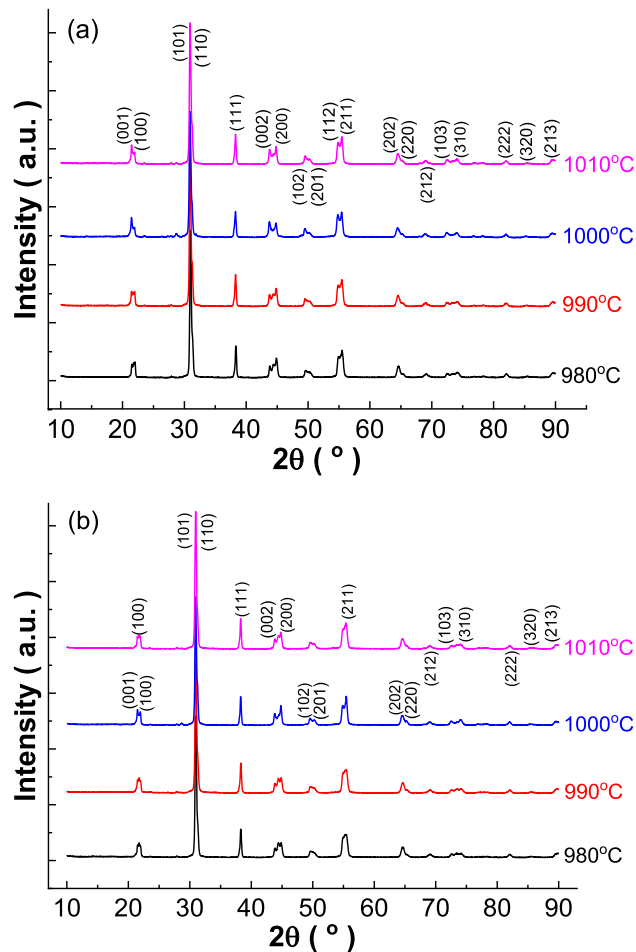


Fig. 2 XRD patterns of BaCW-doped 0.95PZT–0.05BNZ ceramics sintered at low temperatures. **a** 2 wt% BaCW doping; **b** 2.5 wt% BaCW doping

present pure perovskite structure, showing that BNZ second component and BaCW sintering aid can stabilize perovskite structure, form complete solid solution, and realize low-temperature sintering, partially relating to being perovskite structure for both BNZ and BaCW. All BaCW-doped 0.975PZT–0.025BNZ and 0.95PZT–0.05BNZ ceramics present crystal structure dominated by tetragonal phase, in which most diffraction reflections, including {100}, {110}, {200}, {210}, {220}, and {310}, show apparent doublet peaks. With the increase of BaCW doping amount and sintering temperature, although overall XRD patterns remain basically unchanged, the doublet splitting and peak intensity ratio change slightly but have no straightforward change trend. Therefore, the 2 and 2.5 wt% BaCW-doped 0.975PZT–0.025BNZ and 0.95PZT–0.05BNZ ceramics sintered between 980

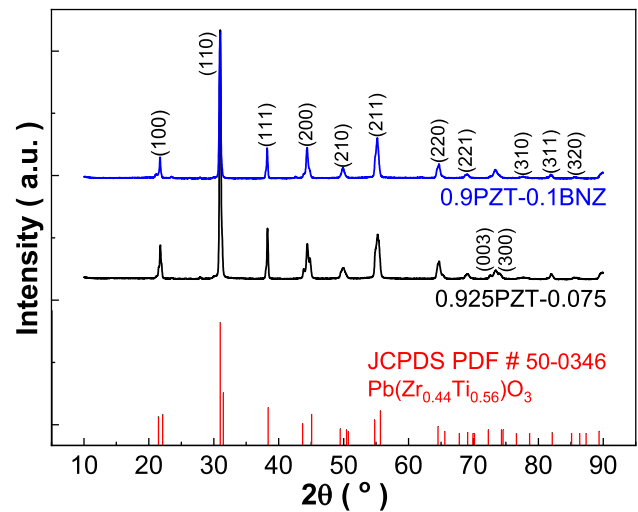


Fig. 3 XRD patterns of 1000 °C sintered 2 wt% BaCW-doped 0.925PZT–0.075BNZ and 0.9PZT–0.1BNZ ceramics

and 1010 °C have tetragonal phase dominant crystal structure.

The influence of $(1-x)$ PZT– x BNZ composition on crystal structure is studied further as shown in Fig. 3. For $x = 0.075$ and $x = 0.1$ compositions, 2 wt% BaCW is added and sintering temperature of 1000 °C is utilized based on analyzing density data of the former samples. The diffraction peaks of all ceramics are indexed according to standard material $\text{Pb}(\text{Zr}_{0.44}\text{Ti}_{0.56})\text{O}_3$ with PDF card 50-0346. All 2 wt% BaCW-doped $(1-x)$ PZT– x BNZ ceramics still exhibit pure perovskite phase without detectable impurity. Combined Figs. 1, 2, and 3 it can be seen, with the increase of BNZ content x , diffraction reflections and peak intensity ratio change gradually for all the 1000 °C sintered ceramics. For the $x = 0.025$ sample, almost all diffraction peaks show doublet splitting peaks, showing mainly tetragonal phase structure. When $x = 0.05$, the high 2θ angle diffraction peaks tend to be broad and singlet peak, showing the appearance of rhombohedral phase in tetragonal matrix. When $x = 0.075$, most diffraction peaks are broad and singlet peak besides the {200} and {300} peaks, revealing that rhombohedral phase becomes main structure feature. For the 2 wt% BaCW-doped 0.9PZT–0.1BNZ sample, most diffraction peaks exhibit sharp, symmetric, and singlet shape besides small broadened peaks {220} and {300}, approaching pure rhombohedral phase. Such structure change mainly relates to tetragonal structure of $\text{Pb}(\text{Zr}_{0.5}\text{Ti}_{0.5})$

O₃ and rhombohedral structure of (Bi_{0.5}Na_{0.5})ZrO₃, and partially correlates with tetragonal structure of Ba(Cu_{0.5}Wu_{0.5})O₃ [12, 18]. XRD characterization confirms successful construction of MPB in the (1-x)PZT-xBNZ ceramics prepared by low-temperature sintering, which is expected to present enhanced electrical properties due to the MPB effect [33].

Based on Jade full XRD pattern refinement, cell parameters are calculated according to tetragonal and rhombohedral phase, respectively, depending on composition as shown in Tables 1 and 2, combining with density measured by water immersion method. Density is an important parameter for piezoelectric materials, and high densification normally predicts excellent electrical performance [34]. For the studied compositions, cell volume and density increase first and then decrease with elevating sintering temperature, exhibiting maximum densification at sintering temperature of 1000 °C. Adding 2 wt% BaCW sintering aid is appropriate, where adding smaller or larger amount sintering aid cannot reduce sintering temperature adequately or maximum relative density is less than 90%. BNZ also promotes sintering, and the largest relative density reaches 96.81% for the 2 wt% BaCW-doped 0.95PZT-0.05BNZ ceramics sintered at 1000 °C. The densification is larger than 93% for the x = 0.075 and x = 0.1 samples, whose optimized sintering temperature may be reduced to below 1000 °C due to more BNZ content in the (1-x)PZT-xBNZ system [35].

3.2 SEM morphology and grain size distribution

Sintering mechanism and morphology characteristics were studied by SEM observation as shown in Fig. 4 using the sample with largest relative density as an example. Although there are some pores-like position, due to free surface used for the SEM measurement, density measurement and performance characterization are not influenced since ceramics are ground and polished. Even sintered at low sintering temperature of 1000 °C, grains grow well, producing clear grain boundary, intact densification, and rather uniform micro-morphology. Due to adding BNZ second component and BaCW sintering aid, liquid-phase sintering mechanism plays major densification role in BaCW-doped (1-x)PZT-xBNZ sintering process since most grains have deformed spherical shape, and there is over-fusion phenomenon as shown by red circle in

Table 1 Unit cell parameters, density, and resistance of 2 wt% BaCW-doped (1-x)PZT-xBNZ ceramics sintered at low temperatures

Composition	Sintering temperature (°C)	a = b (Å)	c (Å)	α = β = γ (°)	Theoretical volume (Å ³)	c/a	Bulk density (g/cm ³)	Theoretical density (g/cm ³)	Relative density (%)	Resistivity (Ωcm)
x = 0.025	980	4.0341	4.1337	90	67.27	1.0247	6.5574	7.9725	82.25	3.8493 × 10 ¹⁰
	990	4.0330	4.1353	90	67.26	1.0254	6.6379	7.9737	83.25	7.7004 × 10 ¹⁰
	1000	4.0395	4.1361	90	67.49	1.0239	7.5346	7.9465	94.82	1.2166 × 10 ¹¹
	1010	4.0343	4.1327	90	67.26	1.0244	7.3391	7.9737	92.04	2.7665 × 10 ¹⁰
x = 0.05	980	4.0341	4.1247	90	67.13	1.0225	6.4378	7.9461	81.02	4.5234 × 10 ¹⁰
	990	4.0352	4.1315	90	67.27	1.0239	6.5600	7.9296	82.73	6.4461 × 10 ¹¹
	1000	4.0397	4.1339	90	67.46	1.0233	7.6550	7.9072	96.81	1.6314 × 10 ¹¹
	1010	4.0383	4.1295	90	67.34	1.0226	7.3709	7.9213	93.05	1.3124 × 10 ¹¹
x = 0.075	1000	4.0761	4.0761	89.734	67.72		7.3217	7.8343	93.46	6.3091 × 10 ¹⁰
x = 0.1	1000	4.0763	4.0763	89.792	67.73		7.2771	7.7905	93.41	1.6804 × 10 ⁹

Table 2 Unit cell parameters, density, and resistance of 2.5 wt% BaCW-doped (1-x)PZT-xBNZ ceramics sintered at low temperatures

Composition	Sintering temperature (°C)	$a=b$ (Å)	c (Å)	$\alpha = \beta = \gamma$ (°)	Theoretical volume (Å ³)	c/a	Bulk density (g/cm ³)	Theoretical density (g/cm ³)	Relative density (%)	Resistivity (Ωcm)
$x=0.025$	980	4.0314	4.1343	90	67.19	1.0255	6.5274	7.9820	81.78	4.6948×10^{10}
	990	4.0346	4.1341	90	67.30	1.0247	6.6067	7.9390	83.62	1.1000×10^{11}
	1000	4.0351	4.1363	90	67.35	1.0251	7.1007	7.9630	89.17	5.3987×10^{10}
	1010	4.0353	4.1356	90	67.34	1.0249	6.8184	7.9642	85.61	2.5413×10^{10}
$x=0.05$	980	4.0384	4.1235	90	67.25	1.0211	6.4141	7.9319	80.87	2.9128×10^{10}
	990	4.0360	4.1246	90	67.19	1.0220	6.6388	7.9390	83.62	1.1146×10^{10}
	1000	4.0398	4.1266	90	67.35	1.0215	7.0596	7.9202	89.13	2.2390×10^{11}
	1010	4.0425	4.1208	90	67.34	1.0194	6.7356	7.9213	85.03	1.5332×10^{10}

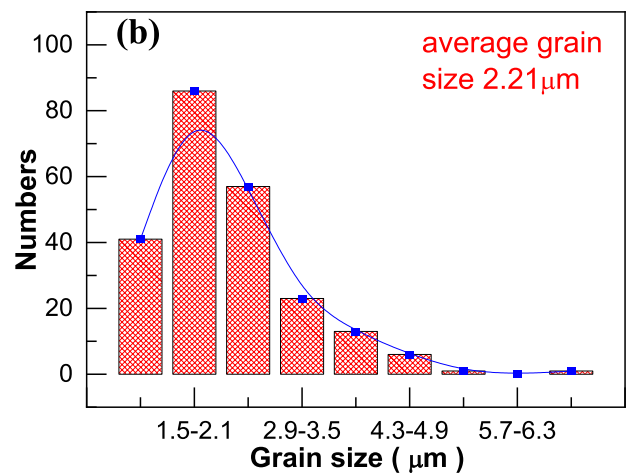
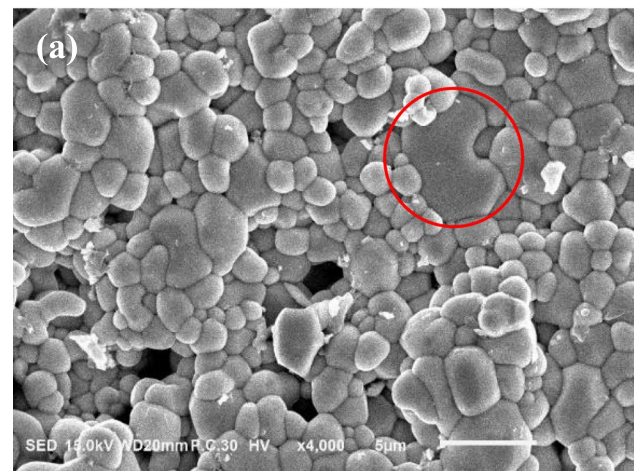
**Fig. 4** SEM photo (a) and grain size statistics (b) of 2 wt% BaCW-doped 0.95PZT-0.05BNZ ceramics sintered at 1000 °C

Fig. 4a [35]. Most grains have grain size of 1.5–2.1 µm, and the average grain size is 2.21 µm, exhibiting narrow grain size distribution. Such grain size is rather small, relating mainly to low-temperature sintering, as compared with several to over ten micrometers for the Pb-based piezoelectric ceramics sintered normally above 1250 °C [4].

3.3 Resistance and dielectric performance

High insulation is fundamental requirement for electrical-related application [30]. As shown in Tables 1 and 2, all BaCW-doped (1-x)PZT-xBNZ ceramics have high resistivity, being larger than 10^9 Ω cm, which are expected to exhibit excellent electrical properties. On the whole, resistivity of the 2 wt% BaCW-doped ceramics is normally larger than that of the 2.5 wt%

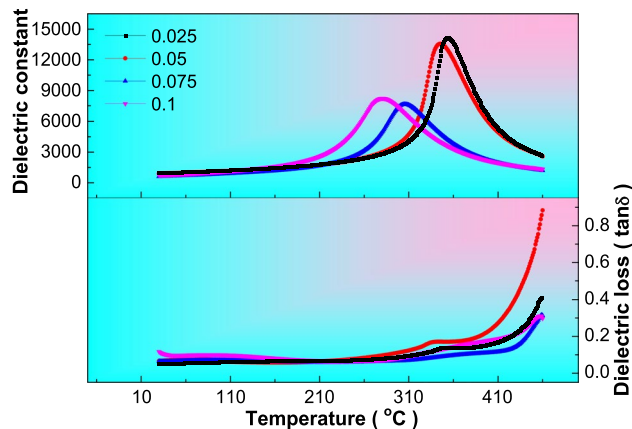


Fig. 5 Temperature dependent dielectric performance at 10 kHz of 2 wt% BaCW-doped $(1-x)$ PZT- x BNZ ceramics sintered at 1000 °C

BaCW-doped ceramics, partially relating to the density change. With elevating sintering temperature, resistivity shows change trend of first increasing and then decreasing, but is not coincidence with the change sequence of relative density. As for the influence of composition, for 2 wt% BaCW doping amount and same sintering temperature, resistivity increases with the increase of x value, reaches maximum value at $x = 0.05$, and then decreases 1–2 magnitude order, respectively, with further increasing the BNZ content to 0.075 and 0.1. The 1000 °C sintered 2 wt% BaCW-doped 0.95PZT–0.05BNZ ceramics have the largest resistivity, being $1.6314 \times 10^{11} \Omega \text{ cm}$. Such complicated resistivity variation relates to many factors, such as composition heterogeneity, density and porosity difference, microstructural morphology, point defects, etc. [32].

For extreme condition application, high T_C temperature is urgently required. Figure 5 shows dielectric properties versus temperature relationship of the 2 wt% BaCW-doped $(1-x)$ PZT- x BNZ ceramics sintered at 1000 °C. For ferroelectrics, spontaneous polarization P_s decreases with the increase of temperature, and ferroelectric phase transition occurs at the T_C temperature at which the P_s value normally decreases to zero accompanied by the appearance of maximum dielectric constant ϵ_m peak [36]. In this work, the ferroelectric phase to paraelectric phase transition is from mainly tetragonal phase, MPB, and mainly rhombohedral phase with elevating the BNT content, to cubic phase. With the increase of BNZ content, dielectric peak changes from narrow to wide shape, T_C

decreases almost linearly from 354 to 280 °C accompanied by decrease of ϵ_m from 14200.9 to 8227.6, and the 2 wt% BaCW-doped 0.95PZT–0.05BNZ sample presents excellent dielectric performance, corresponding well with the structure change from mainly tetragonal phase, across MPB region, and to mainly rhombohedral phase, and revealing the MPB effect [12]. The increased difference between T_C and the temperature of dielectric loss $\tan\delta$ maximum indicates the increase of relaxation degree [16].

Figure 6 compares temperature-dependent dielectric performance at 10 kHz of the 2 and 2.5 wt% BaCW-doped 0.975PZT–0.025BNZ and 0.95PZT–0.05BNZ ceramics, respectively. The sole dielectric peak correlates with tetragonal or MPB ferroelectric phase to cubic paraelectric phase transition. Overall, the 1000 °C sintered ceramics present best dielectric properties, relating to the largest relative density, besides the 1010 °C sintered 2.5 wt% BaCW-doped 0.975PZT–0.025BNZ sample, relating to the largest dielectric loss [37]. The variation of T_C temperature caused by different sintering temperatures is less than 10 °C, but T_C is all higher than 320 °C, showing prospect application in high-temperature and high-power piezoelectric-related fields under extreme condition [4]. Particularly noteworthy is that T_C has little change for the 2 wt% BaCW-doped 0.975PZT–0.025BNZ ceramics sintered at 980–1010 °C, all being around 350 °C.

Figure 7 shows frequency-dependent dielectric properties of 2 wt% BaCW-doped $(1-x)$ PZT- x BNZ ceramics sintered at 1000 °C. The relatively narrow dielectric peaks in BaCW-doped 0.975PZT–0.025BNZ relate to the mainly tetragonal perovskite structure, and the relatively wide dielectric peaks in BaCW-doped 0.9PZT–0.1BNZ correlate with the mainly rhombohedral perovskite structure. Whether in normal ferroelectric state or in relaxor ferroelectric state, the dielectric frequency dispersion is very apparent around the T_C temperature. Overall, the BaCW-doped 0.95PZT–0.05BNZ ceramics show excellent dielectric properties, attributing to the MPB effect [12].

Combined Figs. 5, 6, and 7, it can be seen that dielectric loss $\tan\delta$ increases sharply above the T_C temperature in all ceramics, especially at low frequency of 100 Hz. In piezoelectric materials, dielectric loss is mainly caused by polarization hysteresis loss under alternating current electric field, leakage current induced loss, and defects induced loss correlating with manufacturing process [38]. In this work, the third mechanism dominates the main cause of loss.

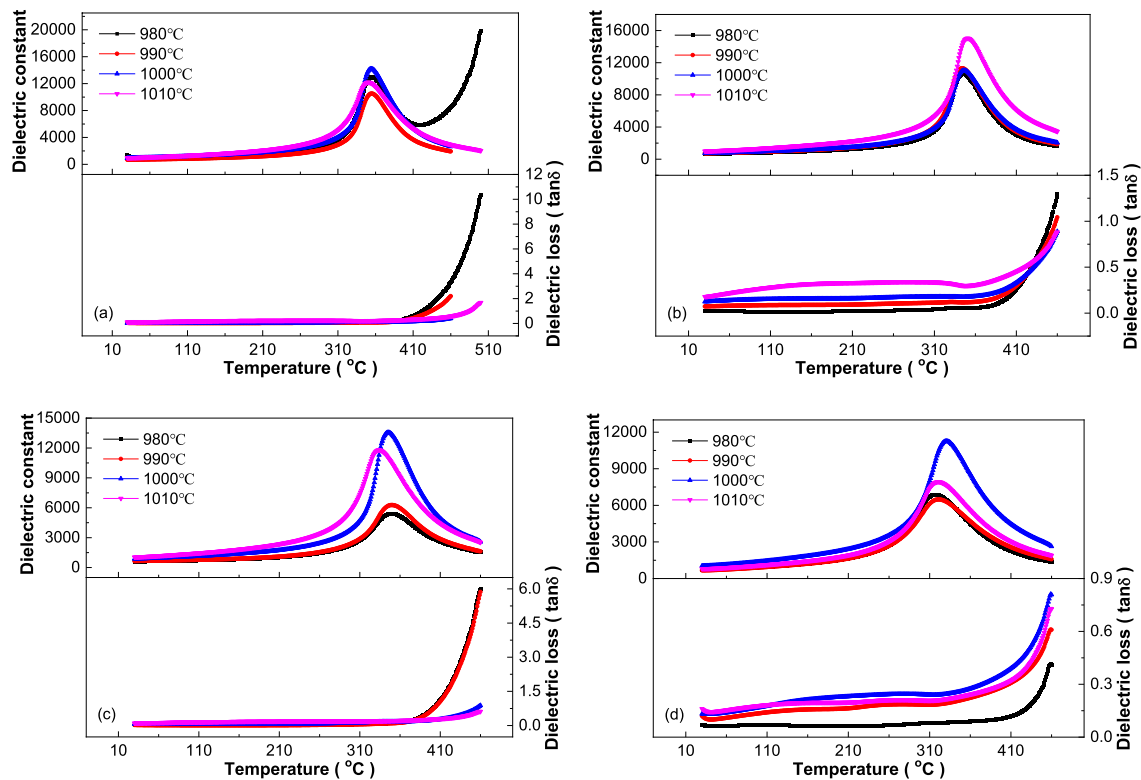
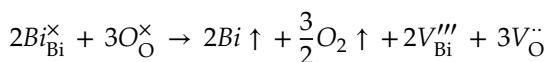
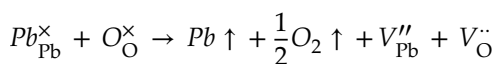


Fig. 6 Influence of sintering temperature on dielectric performance–temperature relationship at 10 kHz of BaCW-doped $(1-x)$ PZT– x BNZ ceramics. **a** 2 wt% BaCW-doped 0.975PZT–

0.025BNZ; **b** 2.5 wt% BaCW-doped 0.975PZT–0.025BNZ; **c** 2 wt% BaCW-doped 0.95PZT–0.05BNZ; **d** 2.5 wt% BaCW-doped 0.95PZT–0.05BNZ

Although low-temperature sintering is realized for preparing the BaCW-doped $(1-x)$ PZT– x BNZ ceramics, the evaporation of Pb^{2+} and Bi^{3+} is inevitable since the melting points of Pb and Bi oxides are still lower than the sintering temperature, resulting in formation of oxygen vacancy defects as shown below [9]:



Such generated oxygen vacancies exhibit typical thermal excitation and lossy-type conductivity characteristic, resulting in sharp increase of leakage current and dielectric loss at high temperatures, especially above the T_C temperature [9].

The frequency dispersion and relaxation characteristic can be studied by dielectric performance fitting as shown in Fig. 8 using exponential law $\frac{1}{\epsilon} - \frac{1}{\epsilon_m} = \frac{(T-T_m)^\gamma}{C}$ [9, 39]. The dielectric behavior

above the T_C temperature of all samples can be fitted well by the exponential law with high fitting accuracy, in which the fitted diffusive coefficient γ of all samples is larger than 1.7, showing high relaxation degree. With the increase of BNZ content, the γ value tends to increase, where BaCW-doped 0.95PZT–0.05BNZ has increased γ , relating to the complicated coexistence of multi-ferroelectric phases around MPB [12]. Such phenomena show that all BaCW-doped $(1-x)$ PZT– x BNZ ceramics have apparent relaxor characteristic whatever in tetragonal or rhombohedral structure, revealing complex influence of forming solid solution on dielectric relaxation characteristic. Important electrical properties are summarized in Tables 3 and 4.

3.4 Ferroelectric and strain properties

Figure 9 compares influence of composition on ferroelectric performance, including polarization–electric field (P – E) hysteresis loops and strain–electric field (S – E) butterfly-like curves, of the 2 wt% BaCW-doped $(1-x)$ PZT– x BNZ ceramics sintered at 1000 °C.

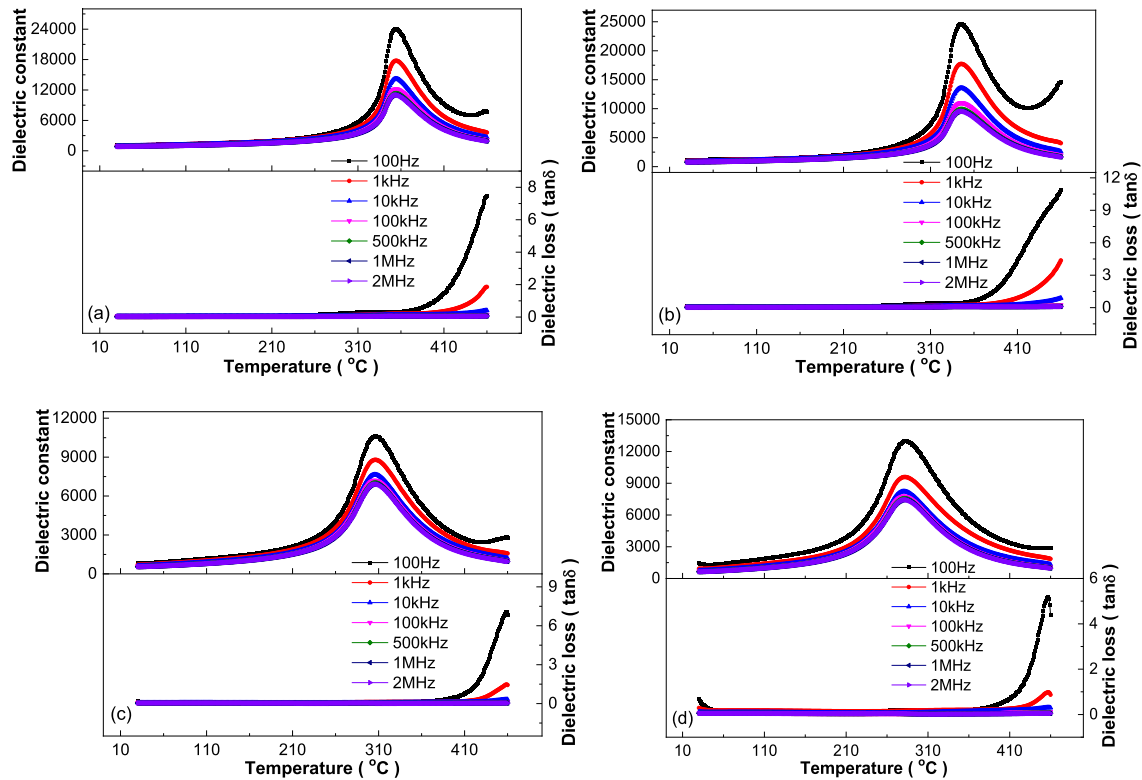


Fig. 7 Influence of frequency on dielectric performance–temperature relationship at 10 kHz of 2 wt% BaCW-doped (1–x)PZT–xBNZ ceramics sintered at 1000 °C. **a** 0.975PZT–0.025BNZ; **b** 0.95PZT–0.05BNZ; **c** 0.925PZT–0.075BNZ; **d** 0.9PZT–0.1BNZ

The normal change from narrow *P–E* loop to nearly rectangular *P–E* loop accompanied by the appearance of extremum values of remnant polarization P_r and coercive field E_c with changing composition across the MPB region is not observed [12]. All *P–E* hysteresis loops of the 1000 °C sintered 2 wt% BaCW-doped (1–x)PZT–xBNZ ceramics are rather saturate and have nearly rectangular shape, in which the P_r and E_c values show increase trend with increasing the BNZ content, and BaCW-doped 0.925PZT–0.075BNZ has the largest P_r , proving that MPB is not composition point but has composition region [10, 13, 14, 33]. BaCW-doped 0.95PZT–0.05BNZ has the largest positive strain and BaCW-doped 0.9PZT–0.1BNZ shows the largest negative strain at 25 kV/cm, and the *S–E* curves are rather symmetric, also reflecting the complex relationship between structure and performance in solid solution.

Influence of sintering temperature on ferroelectricity is shown in Fig. 10. For the 2 wt% BaCW-doped samples, sintering temperature affects ferroelectric performance greatly for both the 0.975PZT–0.025BNZ and 0.95PZT–0.05BNZ compositions, in which the *P–E* loops change from narrow

to nearly rectangular shape accompanied by great increase of the P_r and E_c values with elevating sintering temperature. As comparison, *S–E* performance is affected less besides the 2 wt% BaCW-doped 0.95PZT–0.05BNZ, especially for the 2.5 wt% BaCW-doped 0.975PZT–0.025BNZ and 0.95PZT–0.05BNZ ceramics, almost having no change as sintering temperature increasing. On the whole, maximum positive strain is larger than maximum negative strain for all samples. Slight asymmetry and small breach exist in the *P–E* loops, correlating with frictional resistance-induced energy loss, which is normally caused by polarization rotation, domain wall motion, and especially point defects as discussed above in this work [4, 37].

3.5 Piezoelectric properties

Figure 11 shows piezoelectric constant d_{33} poling electric field relationship of 2 wt% BaCW-doped (1–x)PZT–xBNZ ceramics sintered at 1000 °C. For all samples, the d_{33} values increase almost linearly with the increase of poling electric field. At 2 wt%

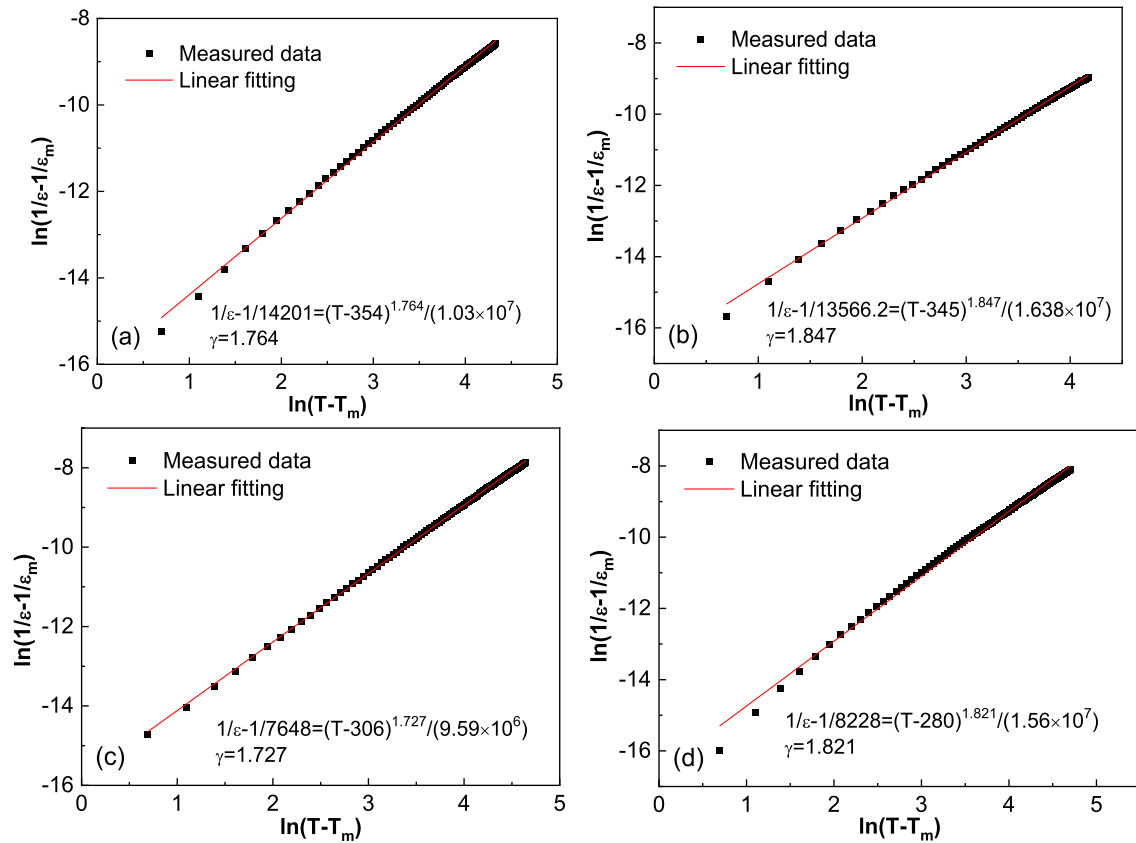


Fig. 8 Exponential law fitting of dielectric characteristic for 2 wt% BaCW-doped (1-x)PZT-xBNZ ceramics sintered at 1000 °C at 10 kHz. **a** 0.975PZT-0.025BNZ; **b** 0.95PZT-0.05BNZ; **c** 0.925PZT-0.075BNZ; **d** 0.9PZT-0.1BNZ

Table 3 Important dielectric properties, and piezoelectric performance poled under 25 kV/cm of 2 wt% BaCW-doped (1-x)PZT-xBNZ ceramics sintered at low temperatures

Composition	Sintering temperature (°C)	ϵ_m (100 Hz)	T_m (°C, 100 Hz)	ϵ_m (2 MHz)	T_m (°C, 2 MHz)	ΔT (°C, 100 Hz-2 MHz)	Diffuseness coefficient (γ , 10 kHz)	d_{33} (pC/N)	K_p	Q_m
$x=0.025$	980	12,997	355	8185	357	2	1.859	78	0.114	111.1
	990	14,761	355	8996	355	0	1.737	106	0.199	76.5
	1000	24,047	354	11,012	354	0	1.764	103	0.168	71.2
	1010	35,889	351	9518	350	-1	1.651	120	0.203	72.4
$x=0.05$	980	7856	348	4852	349	1	1.921	43	0.111	111.1
	990	8870	349	5562	350	1	1.811	45	0.093	155.2
	1000	24,592	345	9546	345	0	1.847	151	0.221	79.4
	1010	30,454	335	9174	333	-2	1.710	159	0.221	78.5
$x=0.075$	1000	10,598	306	6917	306	0	1.727	121	0.234	52.4
$x=0.1$	1000	12,972	281	7434	282	1	1.821	209	0.191	45.1

Table 4 Important dielectric properties, and piezoelectric performance poled under 25 kV/cm of 2.5 wt% BaCW-doped (1-x)PZT-xBNZ ceramics sintered at low temperatures

Composition	Sintering temperature (°C)	ϵ_m (100 Hz)	T_m (°C, 100 Hz)	ϵ_m (2 MHz)	T_m (°C, 2 MHz)	ΔT (°C, 100 Hz-2 MHz)	Diffuseness coefficient (γ , 10 kHz)	d_{33} (pC/N)	K_p	Q_m
x=0.025	980	13,293	345	9399	346	1	1.807	146	0.187	87.2
	990	17,821	343	9389	345	2	1.753	159	0.204	86.3
	1000	21,904	346	8677	347	1	1.768	157	0.207	97.7
	1010	50,434	350	10,350	350	0	1.630	162	0.184	97.9
x=0.05	980	9387	317	6031	317	0	1.831	151	0.187	72.8
	990	16,362	323	5199	321	- 2	1.792	152	0.167	79.9
	1000	31,956	332	8044	330	- 2	1.654	154	0.205	80.4
	1010	20,617	322	6100	320	- 2	1.707	154	0.188	87.4

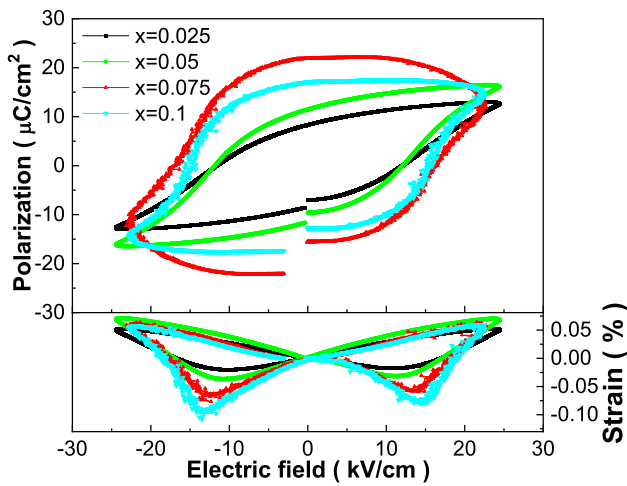


Fig. 9 P-E hysteresis loops and S-E curves of 2 wt% BaCW-doped (1-x)PZT-xBNZ ceramics sintered at 1000 °C

BaCW doping amount sintering aid and same sintering temperature, 0.9PZT-0.1BNZ presents extra-large piezoelectricity of $d_{33} = 209$ pC/N, whose T_C is only 281 °C. The relatively large d_{33} of 151 pC/N for 0.95PZT-0.05BNZ also attributes to the MPB effect [10, 33], whose T_C is high as 345 °C.

Figure 12 shows the influence of sintering temperature on piezoelectric performance for 2 systems of BaCW-doped (1-x)PZT-xBNZ ceramics. Overall, the 2.5 wt% BaCW-doped samples have higher d_{33} value as compared with the 2 wt% BaCW-doped samples with same (1-x)PZT-xBNZ composition. Higher sintering temperature tends to induce larger piezoelectric constant, but the difference becomes almost negligible at higher poling electric field of 25 kV/cm, besides the 2 wt% BaCW-doped 0.95PZT-0.05BNZ.

Under 25 kV/cm poling electric field, the 1010 °C sintered 2.5 wt% BaCW-doped 0.975PZT-0.025BNZ ceramics achieve the largest d_{33} value of 163 pC/N. The complicated change of piezoelectricity with composition, sintering temperature, and poling electric field partially relates to uniformity change of ceramics caused by sublimation of Pb and Bi during sintering [9, 26].

Figure 13 shows impedance and phase angle resonance curves using the 1000 °C sintered 2 wt% BaCW-doped (1-x)PZT-xBNZ ceramics poled under 25 kV/cm as examples. All curves have excellent resonant and anti-resonant characteristics, providing effective energy conversion between mechanical energy and electrical energy. Based on Fig. 13 and according to formulae $K_p \approx \sqrt{\frac{f_p - f_s}{f_s}} \times 2.33$ and $Q_m = \frac{f_p^2}{2\pi \cdot f_s \cdot C^T \cdot R(f_p^2 - f_s^2)}$ [26], electromechanical coupling coefficient K_p and mechanical quality factor Q_m are obtained as shown in Tables 3 and 4. Overall, higher density samples have larger K_p . The phase angle θ is normally less than 50°, showing possibility to improve poling effect by other poling techniques, such as alternating current poling [40]. The Q_m value is around several dozens or slightly larger than 100, being typical soft piezoelectric materials, and relating to generation of oxygen vacancies due to evaporation of Pb and Bi during sintering [9, 26]. The high T_C temperature combined with acceptable piezoelectric performance studied in the (1-x)PZT-xBNZ system prepared by low-temperature sintering via adding BaCW sintering aid shows prospect application in extreme high-temperature piezoelectric-related fields.

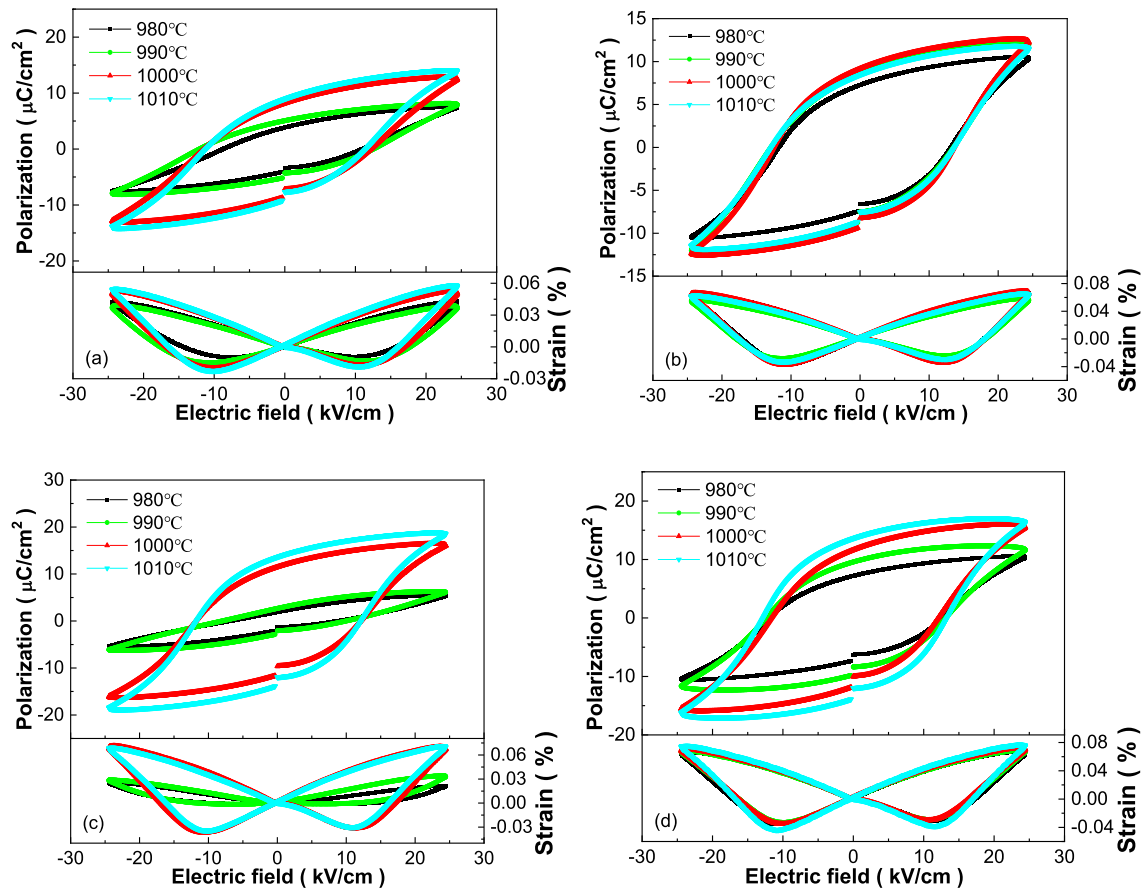


Fig. 10 Relationship of piezoelectric constant d_{33} versus poling electric field of 2 wt% BaCW-doped $(1-x)$ PZT- x BNZ ceramics sintered at 1000 °C

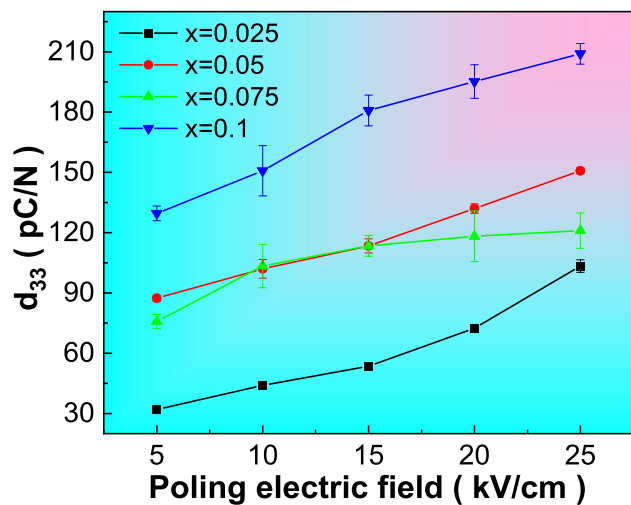


Fig. 11 Poling electric field-dependent piezoelectricity of BaCW-doped $(1-x)$ PZT- x BNZ ceramics sintered at low temperatures

4 Conclusions

Low-temperature densified sintering was realized in the $(1-x)$ PZT- x BNZ system at around 1000 °C sintering temperature due to adding BNZ second component and BaCW sintering aid. All sintered BaCW-doped $(1-x)$ PZT- x BNZ ceramics present pure perovskite structure, which changes from mainly tetragonal phase, across MPB region and to mainly rhombohedral phase with increasing the BNZ content. High density ceramics are obtained at low sintering temperature, which present decreased grain size, narrowed grain size distribution, and enhanced homogenous morphology, mainly relating to low-temperature sintering. The 2 wt% BaCW-doped 0.95PZT-0.05BNZ ceramics sintered at 1000 °C achieve the largest relative density of 96.81%. All BaCW-doped $(1-x)$ PZT- x BNZ ceramics have

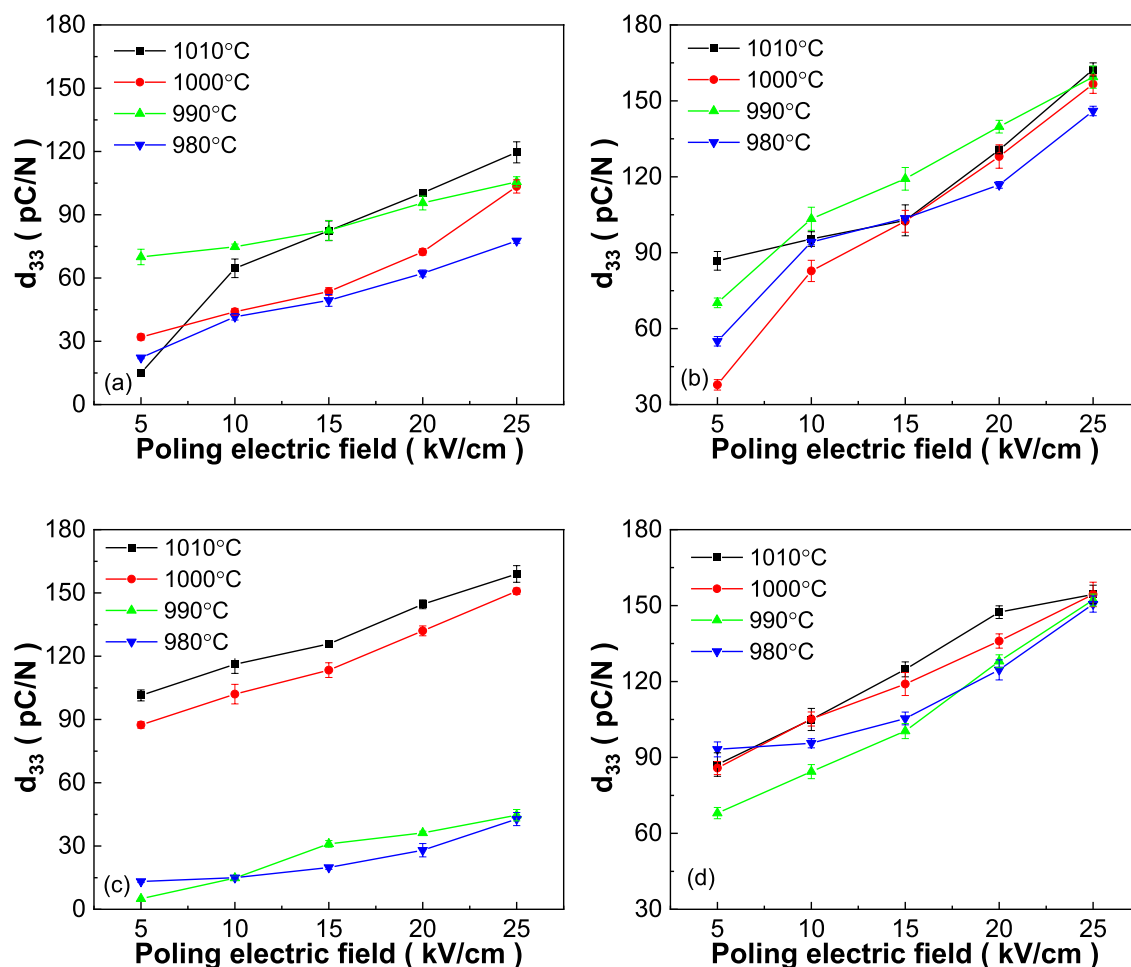


Fig. 12 Change of phase angle and impedance with frequency of 2 wt% BaCW-doped $(1-x)$ PZT- x BNZ ceramics sintered at 1000 °C poled under 25 kV/cm. **a** 2 wt% BaCW-doped 0.975PZT-

0.025BNZ; **b** 2.5 wt% BaCW-doped 0.975PZT-0.025BNZ; **c** 2 wt% BaCW-doped 0.95PZT-0.05BNZ; **d** 2.5 wt% BaCW-doped 0.95PZT-0.05BNZ

high resistivity larger than $10^9 \Omega \text{ cm}$, and the MPB effect is confirmed in dielectric, ferroelectric, and piezoelectric properties. The 1000 °C sintered 2 wt% BaCW-doped 0.95PZT-0.05BNZ ceramics have the largest resistivity of $1.6314 \times 10^{11} \Omega \text{ cm}$. All samples have apparent relaxation characteristic whatever in tetragonal or rhombohedral structure, and the diffusive coefficient γ increases with elevating the BNZ content, revealing complex influence of forming solid solution on electrical properties. The 1000 °C sintered 2 wt% BaCW-doped $(1-x)$ PZT- x BNZ ceramics have rather saturate and nearly rectangular shape P - E loops, in which the P_r and E_c values show increase trend with increasing the BNZ

content. The 1000 °C sintered 2 wt% BaCW-doped 0.9PZT-0.1BNZ has $d_{33} = 209 \text{ pC/N}$ with $T_C = 281 \text{ }^\circ\text{C}$ and 0.95PZT-0.05BNZ has $d_{33} = 151 \text{ pC/N}$ with $T_C = 345 \text{ }^\circ\text{C}$. The low-temperature sintered BaCW-doped $(1-x)$ PZT- x BNZ ceramics exhibit broad application prospect in high-temperature piezoelectric-related fields due to the high T_C temperature and acceptable piezoelectric performance.

Author contributions

BF contributed toward conceptualization; BF and JD contributed toward supervision; HL, BF and JD contributed toward methodology; HL and SZ contributed

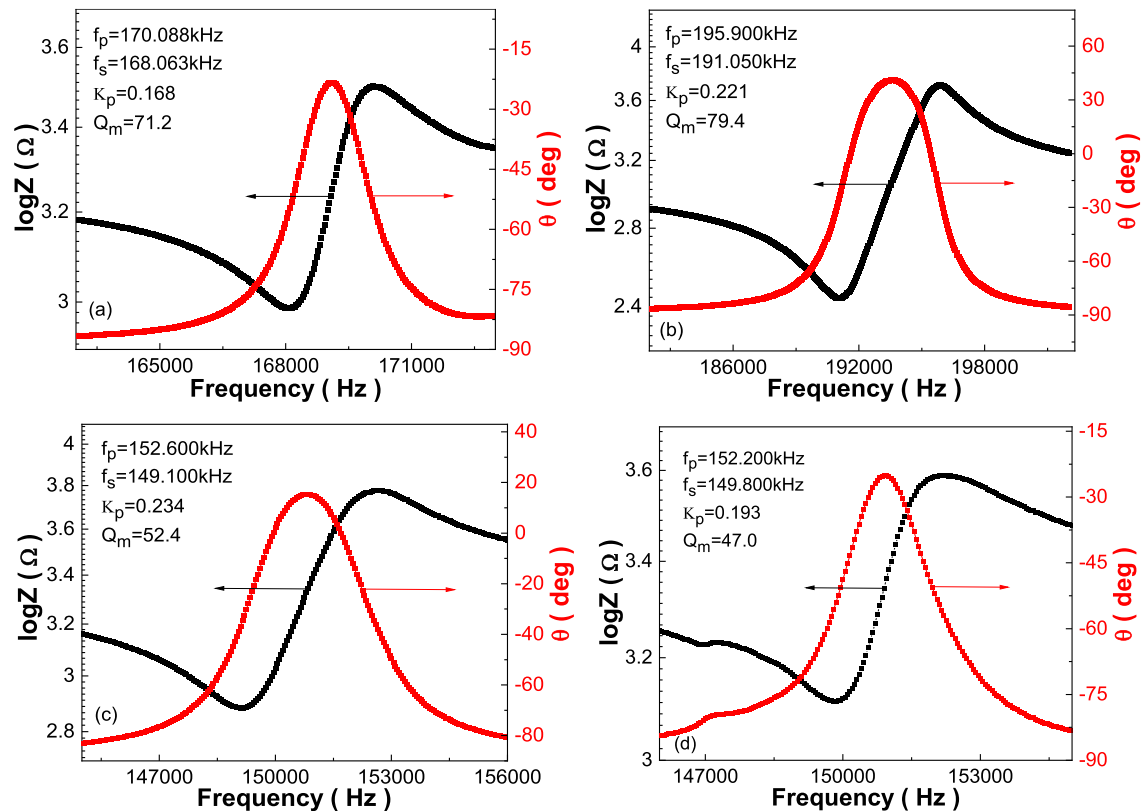


Fig. 13 Change of phase angle and impedance with frequency of 2 wt% BaCW-doped $(1-x)\text{PZT}-x\text{BNZ}$ ceramics sintered at $1000\text{ }^\circ\text{C}$ poled under 25 kV/cm . **a** 0.975PZT–0.025BNZ; **b** 0.95PZT–0.05BNZ; **c** 0.925PZT–0.075BNZ; **d** 0.9PZT–0.1BNZ

toward formal analysis; HL, SZ, and XL contributed toward investigation; HL and XL contributed toward data curation; HL and BF contributed toward writing—original draft; BF contributed toward Writing—review and editing. All authors have read and agreed to the published version of the manuscript.

Funding

This work was supported by the Top-notch Academic Programs Project of Jiangsu Higher Education Institutions and the Priority Academic Program Development of Jiangsu Higher Education Institutions.

Data availability

All data that support the findings of this study are included within the article.

Declarations

Conflict of interest The authors declare that they have no known competing financial interests or personal relationships that could have appeared to influence the work reported in this paper.

References

1. J.-H. Lee, G.-J. Lee, A.-P. Hoang, T. Frömling, T.-L. Pham, J.-S. Lee, W. Jo, *J. Eur. Ceram. Soc.* **42**, 1388–1395 (2022)
2. P. Li, J. Zhai, B. Shen, S. Zhang, X. Li, F. Zhu, X. Zhang, *Adv. Mater.* **30**, 1705171 (2018)
3. X. He, B. Fang, S. Zhang, X. Lu, J. Ding, *J. Alloys Compd.* **925**, 166249 (2022)
4. L. Chen, H. Liu, H. Qi, J. Chen, *Prog Mater. Sci.* **127**, 100944 (2022)

5. Z. Liu, H. Wu, Y. Yuan, H. Wan, Z. Luo, P. Gao, J. Zhuang, J. Zhang, N. Zhang, J. Li, Y. Zhan, W. Ren, Z.-G. Ye, *Curr. Opin. Solid State Mater. Sci.* **26**, 101016 (2022)
6. T.Y. Ansell, D.P. Cann, E. Sapper, J. Rödel, *J. Am. Ceram. Soc.* **98**, 455–463 (2015)
7. Y. Wang, H. Ma, G. Yuan, H. Luo, D. Viehland, *J. Am. Ceram. Soc.* **100**, 1751–1759 (2017)
8. J. Chen, J. Li, L. Fan, N. Zou, P. Ji, L. Liu, L. Fang, H. Kang, X. Xing, *J. Appl. Phys.* **112**, 1–7 (2012)
9. W. Ji, S. Feng, B. Fang, X. Zhao, S. Zhang, J. Ding, H. Luo, *Curr. Appl. Phys.* **18**, 289–296 (2018)
10. T. Zhao, C. Fei, K. Pu, X. Dai, J. Song, C. Wang, S. Dong, *J. Alloys Compd.* **873**, 159844 (2021)
11. Y. Wei, C. Bai, C. Jin, W. Zhu, Z. Jian, R. Nan, L. Hu, Z. Dai, *J. Mater. Sci.* **56**, 11838–11846 (2021)
12. E. Hou, Y. Yan, M. Zhang, D. Zhang, Z. Li, *Ceram. Int.* **46**, 27394–27400 (2020)
13. Y. Yang, C. Liu, Y. Ji, L. He, X. Ren, *Acta Mater.* **208**, 116720 (2021)
14. S.R. Maity, B. Tiwari, M. Rath, M.S. Ramachandra Rao, *J. Solid State Chem.* **325**, 124131 (2023)
15. F. Luo, H.W. Guan, R. Peng, J. Jian, J.G. Chen, J.R. Cheng, *J. Am. Ceram. Soc.* **102**, 5958–5965 (2019)
16. J. Zidani, M. Zannen, M. Hadouchi, H.A.H. Alzahrani, E. Birks, H. Khemakhem, M. Majdoub, A. Lahmar, *Phys. B* **653**, 414680 (2023)
17. X. Lv, N. Zhang, J. Wu, X. Zhang, *Acta Mater.* **197**, 224–234 (2020)
18. P. Li, Z. Fu, F. Wang, Y. Huan, Z. Zhou, J. Zhai, B. Shen, S. Zhang, *Acta Mater.* **199**, 542–550 (2020)
19. K. Batra, N. Sinha, B. Kumar, *J. Phys. Chem. Solids.* **170**, 110953 (2022)
20. M.A. Beuerlein, N. Kumar, T.-M. Usher, H.J. Brown-Shaklee, N. Raengthon, I.M. Reaney, D.P. Cann, J.L. Jones, G.L. Brennecke, *J. Am. Ceram. Soc.* **99**, 2849–2870 (2016)
21. K. Liu, Y. Xia, Q. Zhang, Y. Du, Y. Shi, S. Joshi, C. Yan, Y. Wu, S. Huang, H. Sun, *Ceram. Int.* **49**, 20024–20033 (2023)
22. J. Lin, B. Cui, J. Cheng, Q. Tan, J. Chen, *Ceram. Int.* **49**, 474–479 (2023)
23. K. Li, E. Sun, Y. Zhang, Z. Song, X. Qi, Y. Sun, J. Li, B. Yang, J. Liu, W. Cao, *J. Mater. Chem.* **9**, 2426–2436 (2021)
24. E. Chandrakala, J.P. Praveen, B.K. Hazra, D. Das, *Ceram. Int.* **42**, 4964–4977 (2016)
25. R. Zhu, B. Fang, X. Zhao, S. Zhang, D. Wu, J. Ding, *J. Eur. Ceram. Soc.* **38**, 1463–1472 (2018)
26. L. Tan, X. Wang, W. Zhu, A. Li, Y. Wang, *J. Alloy Compd.* **874**, 159770 (2021)
27. L. Zhao, B. Zhang, W. Wang, Y. Ding, S. Zhang, L. Zhu, N. Wang, *Ceram. Int.* **42**, 7366–7372 (2016)
28. Y. Ying, X. Xiong, N. Wang, J. Zheng, J. Yu, W. Li, L. Qiao, W. Cai, J. Li, H. Huang, S. Che, *J. Eur. Ceram. Soc.* **41**, 5924–5930 (2021)
29. X. Wang, H.L. Chan, C. Choy, *J. Am. Ceram. Soc.* **86**, 1809–1811 (2003)
30. W. Li, X. Liu, J. Ma, Y. Wu, Y. Cui, *J. Mater. Sci. Mater. Electron.* **24**, 1551–1555 (2013)
31. T. Avani Babu, W. Madhuri, *Chem. Phys. Lett.* **799**, 139641 (2022)
32. Y. Zhou, B. Fang, S. Zhang, X. Lu, J. Ding, *J. Korean Ceram. Soc.* **59**, 551–564 (2022)
33. D. Lin, S. Zhang, E. Gorzkowski, S. Zhou, W. Liu, F. Li, *J. Eur. Ceram. Soc.* **37**, 2813–2823 (2017)
34. K. Tsuji, A. Ndayishimiye, S. Lowum, R. Floyd, K. Wang, M. Wetherington, J. Maria, C.A. Randall, *J. Eur. Ceram. Soc.* **40**, 1280–1284 (2020)
35. R.M. German, P. Suri, S.J. Park, *J. Mater. Sci.* **44**, 1–39 (2009)
36. K. Xu, J. Li, X. Lv, J. Wu, X. Zhang, D. Xiao, J. Zhu, *Adv. Mater.* **28**, 8519–8523 (2016)
37. T. Zheng, J. Wu, D. Xiao, J. Zhu, *Prog. Mater. Sci.* **98**, 552–624 (2018)
38. Y. Wang, W. Jie, C. Yang, X. Wei, J. Hao, *Adv. Funct. Mater.* **29**, 1808118 (2019)
39. K. Uchino, S. Nomura, *Ferroelectr. Lett.* **44**, 55–61 (1982)
40. H. Wan, C. Luo, C. Chung, Y. Yamashita, X. Jiang, *Appl. Phys. Lett.* **118**, 102904 (2021)

Publisher's Note Springer Nature remains neutral with regard to jurisdictional claims in published maps and institutional affiliations.

Springer Nature or its licensor (e.g. a society or other partner) holds exclusive rights to this article under a publishing agreement with the author(s) or other rightsholder(s); author self-archiving of the accepted manuscript version of this article is solely governed by the terms of such publishing agreement and applicable law.